Prediction of the Permeability of Fibrous Porous Media Using the Lattice Boltzmann Method in Conjuction with Coarse Numerical Lattices

Martin L.R. Thomas*, Derk B. Ingham and Mohamed Pourkashanian

Centre for Computational Fluid Dynamics, University of Leeds, Leeds, LS2 9JT, UK

Abstract: In this study the lattice Boltzmann method (LBM) is used to simulate Stokes flow through unimodal fibrous porous media. A systematic analysis is carried out to determine the suitability of the LBM to predict the permeability of such porous media using relatively coarse numerical lattices. The discretization of fibres using the LBM is discussed in detail with respect to the introduced errors. Subsequently the LBM is calibrated with the aim of compensating for the dominant error terms. For this purpose, simulations of the flow through simple square arrays of parallel cylinders are carried out for fibre-discretizations up to a radius of six lattice units and for solid volume fractions (SVFs) ranging from 0.1 to 0.4. The results obtained are compared to literature data to obtain an estimate for the dominant error terms. Employing the idea of an effective hydrodynamic radius, the error estimates can be taken into account when modeling fibrous porous media. To assess the suitability of this approach, computations for the flow through random arrays of parallel fibres and for random disordered fibrous media are carried out and the predicted permeabilities are compared with literature data. For small SVF, $\leq$ 0.2, the LBM predictions are found to agree well with literature data even for very coarse lattices. At higher SVF the accuracy of the method quickly deteriorates.

Keywords: LBM, MRT, TRT, fibrous porous media, permeability.

1. INTRODUCTION

The problem of determining the hydraulic permeability of microstructured fibrous porous media is common to many different application areas such as fuel cells, textiles, composite materials or filtration processes (e.g. [1-3]). The existing approaches vary greatly with respect to the required input data, flexibility with regard to the considered micro structure, accuracy and required computational effort. In general one can distinguish between analytical methods that describe the permeability of a porous medium as a function of other, usually geometric, properties of the medium, and numerical methods that solve for some type of transport equation to obtain an estimate for the permeability. Analytical expressions are usually limited in their validity to specific types of porous media, such as beds of spheres or fibrous porous media. Numerical methods on the other hand are usually very flexible and can predict the permeability over a wide range of porous media. The major drawbacks of numerical methods are the relatively complex procedure of carrying out the analysis and the generally high computational costs. The lattice Boltzmann method (LBM) considered in this study is a common numerical method to simulate the flow through fibrous porous media (e.g. [4-6]). The LBM does not directly solve for the governing macroscopic transport equations. Instead, it employs a gas kinetic approach which allows to recover the macroscopic transport equations. One advantage over other numerical methods is that the gas kinetic approach can be implemented using a numerical lattice and nearest neighbour dynamics. This results in the computational costs of LBM simulations to scale practically linearly with the number of lattice nodes. The computational cost of other methods such as finite volume or finite element methods, usually increases at a much higher rate with increasing domain size [7]. The LBM is therefore especially suited for computations involving very large domains. Furthermore, in contrast to many other numerical methods, the LBM does not require a geometry-fitted mesh. Instead it uses a regular lattice for spatial discretization. Using the so-called full bounce-back (FBB) algorithm to model no-slip boundaries (see for example [8]), the geometry definition is reduced to defining nodes as being either solid or fluid. This allows complex geometries to be modeled with ease and allows for a fully automated simulation procedure, reducing the previously mentioned drawback of complex procedures usually required when using numerical methods. At the same time, the LBM is computationally expensive. To accurately simulate the flow through fibrous porous media the mesh has to be sufficiently fine and this can easily result in the computational cost being prohibitive. It would therefore be desirable to be able to achieve a sufficient accuracy of the LBM on relatively coarse lattices. More sophisticated no-slip boundary conditions have been developed ([9] and references therein) that are more accurate than the FBB boundary condition but at the cost of a more complicated geometry definition. Instead, the FBB boundary condition is employed in this paper and the suitability of calibrating the LBM for the special case of fibrous porous media to increase its accuracy is assessed.

2. DESCRIPTION OF THE MRT LATTICE-BOLTZMANN METHOD

Lattice Boltzmann methods can be seen as discrete methods to solve the Boltzmann equation [10], based upon a

*Address correspondence to this author at the Centre for Computational Fluid Dynamics, University of Leeds, Leeds, LS2 9JT, UK; Tel: +44 (0) 1133433824; Fax: +44 (0) 1132467310; E-mail: mlrthomas@gmail.com

1877-7295/10

simplified phase space. The LBM used in this study furthermore approximates the unsteady, incompressible Navier-Stokes equations. In contrast to many other CFD methods, the LBM is based on kinetic theory rather than continuum theory. The LBM is an inherently unsteady method and each time step is usually divided into a collision step and a streaming step. The collision step is completely local while the streaming step involves nearest neighbours where information is passed on from one node to the next along the so called lattice links. While the streaming step is the same for most LBMs, there exist many different forms of the collision step, called collision operators. The LBM employed in this study is described in the next paragraph, including the relevant boundary conditions.

2.1. Discrete Phase Space

Usually a regular lattice is used to discretizise the lattice Boltzmann equation (LBE) in space, with a uniform lattice spacing of δx. A set of vectors, called lattice links, connect each lattice node with some or all of its neigbouring nodes and these are denoted $\mathbf{e}$. At each time step δt, information is passed from each node to the nodes it is connected to. On each lattice site the velocity space is discretizised using a finite set of Q velocity vectors ξ_i, $i = 1, ...Q$. In the scope of the LBM, the velocity space discretizations are usually denoted $DxQy$, where x stands for the number of spatial dimensions and y for the number of discrete velocity vectors Q. In this work a $D3Q19$ model is used. With the exception of the zero velocity vector, the ξ_i and $\mathbf{e_i}$ have the same spatial orientation and the magnitude of the velocity vectors is determined by the length of the corresponding lattice link divided by the time step size. Both the lattice links and the non-zero velocity vectors are identified by the index i which ranges from 1 to $Q-1$.

2.2. Discrete Boltzmann Equation

For the LBM, the Boltzmann equation requires to be discretized on each lattice node. With $\mathbf{r}$ being the position vector of a certain lattice node and with t being a specific point in time, the resulting lattice Boltzmann equation can be written as follows:

$$f_i(\mathbf{r}+\xi_i\cdot\delta t, t+\delta t) = f_i(\mathbf{r},t) + \delta t\cdot\Omega\left(F_i(\mathbf{r},t) f_i(\mathbf{r},t)\right), \tag{1}$$

where f_i represents the discrete velocity distribution function and Ω denotes the collision operator. The collision operator describes the relaxation of the f_i towards equilibrium. Ω is a function of the discrete equilibrium velocity distribution function F_i:

$$F_i(\mathbf{r},t) = w_i\rho\left[1+\frac{\mathbf{e_i u}}{c_S^2}+\frac{\left(\mathbf{e_i u}\right)^2}{2c_S^4}-\frac{\mathbf{u}\cdot\mathbf{u}}{2c_S^2}\right] \tag{2}$$

Here ρ denotes the fluid density, $\mathbf{u}$ the macroscopic velocity vector, c_S the lattice speed of sound and w_i are weighting factors. For the three-dimensional 19-velocity (D3Q19) model used in this study, $\mathbf{e_i}$ and w_i are given as follows:

$$\mathbf{e_i} = \begin{cases} (0,0,0) & \text{for } i = 0 \\ (-1,0,0),(0,-1,0),(0,0,-1) & \text{for } i = 1-6 \\ (-1,-1,0),(-1,0,-1),(0,-1,-1) & \text{for } i = 7-18 \end{cases} \tag{3}$$

$$w_i = \begin{cases} 1/3 & \text{for } i = 0 \\ 1/18 & \text{for } i = 1-6 \\ 1/36 & \text{for } i = 7-18 \end{cases} \tag{4}$$

From the velocity distribution functions f_i, all macroscopic properties of the fluid can be derived ([10]). The macroscopic properties can be defined as so called moments of the velocity distribution functions. In general, a moment m is defined using an arbitrary function $\Psi(\xi)$:

$$m = \sum_{i=0}^{i=Q} f_i(\mathbf{r},t)\cdot\Psi(\xi) \tag{5}$$

By choosing the appropriate functions $\Psi(\xi)$, the according moments yield different macroscopic quantities. The two basic moments for mass and momentum can be written as follows:

$$\rho(\mathbf{r},t) = \sum_{i=0}^{i=Q} f_i(\mathbf{r},t) \tag{6}$$

$$\rho\cdot\mathbf{u}(\mathbf{r},t) = \sum_{i=0}^{i=Q} \xi_i f_i(\mathbf{r},t) \tag{7}$$

For incompressible flow, in LBM notation, the pressure p is calculated using an equation of state [11], that in the case of the lattice considered here reduces to the following expression:

$$p = \frac{\rho}{3} \tag{8}$$

The viscosity of the simulated fluid in LBM notation is given by the following expression [11]:

$$\nu = \frac{(2\tau-1)}{6} \tag{9}$$

where τ is the relaxation rate or relaxation frequency.

2.3. MRT/TRT Collision Operator

The collision operator models the interactions between the molecules of the fluid and determines at which rate the distribution functions f_i relax towards their local equilibrium F_i. A very popular collision operator is based on the assumption of a constant relaxation rate that applies to all f_i. This collision operator is known as the single-relaxation time (SRT) or Baghnar-Gross-Krook (BGK) operator. One major drawback of this operator with respect to the prediction of the permeabilities of porous media is that the exact position of the modeled fluid/solid interface changes if the lattice viscosity changes. This results in an apparent viscosity dependence of the predicted permeability ([9]). This shortcoming of the LBM can be overcome by using different relaxation rates for the different f_i ([9-12]). This

$$\mathbf{M} = \begin{bmatrix}
1 & 1 & 1 & 1 & 1 & 1 & 1 & 1 & 1 & 1 & 1 & 1 & 1 & 1 & 1 & 1 & 1 & 1 & 1 \\
-30 & -11 & -11 & -11 & 8 & 8 & 8 & 8 & 8 & 8 & -11 & -11 & -11 & 8 & 8 & 8 & 8 & 8 & 8 \\
12 & -4 & -4 & -4 & 1 & 1 & 1 & 1 & 1 & 1 & -4 & -4 & -4 & 1 & 1 & 1 & 1 & 1 & 1 \\
0 & -1 & 0 & 0 & -1 & -1 & -1 & -1 & 0 & 0 & 1 & 0 & 0 & 1 & 1 & 1 & 1 & 0 & 0 \\
0 & 4 & 0 & 0 & -1 & -1 & -1 & -1 & 0 & 0 & -4 & 0 & 0 & 1 & 1 & 1 & 1 & 0 & 0 \\
0 & 0 & -1 & 0 & -1 & 1 & 0 & 0 & -1 & -1 & 0 & 1 & 0 & 1 & -1 & 0 & 0 & 1 & 1 \\
0 & 0 & 4 & 0 & -1 & 1 & 0 & 0 & -1 & -1 & 0 & -4 & 0 & 1 & -1 & 0 & 0 & 1 & 1 \\
0 & 0 & 0 & -1 & 0 & 0 & -1 & 1 & -1 & 1 & 0 & 0 & 1 & 0 & 0 & 1 & -1 & 1 & -1 \\
0 & 0 & 0 & 4 & 0 & 0 & -1 & 1 & -1 & 1 & 0 & 0 & -4 & 0 & 0 & 1 & -1 & 1 & -1 \\
0 & 2 & -1 & -1 & 1 & 1 & 1 & 1 & -2 & -2 & 2 & -1 & -1 & 1 & 1 & 1 & 1 & -2 & -2 \\
0 & -4 & 2 & 2 & 1 & 1 & 1 & 1 & -2 & -2 & -4 & 2 & 2 & 1 & 1 & 1 & 1 & -2 & -2 \\
0 & 0 & 1 & -1 & 1 & 1 & -1 & -1 & 0 & 0 & 0 & 1 & -1 & 1 & 1 & -1 & -1 & 0 & 0 \\
0 & 0 & -2 & 2 & 1 & 1 & -1 & -1 & 0 & 0 & 0 & -2 & 2 & 1 & 1 & -1 & -1 & 0 & 0 \\
0 & 0 & 0 & 0 & 1 & -1 & 0 & 0 & 0 & 0 & 0 & 0 & 0 & 1 & -1 & 0 & 0 & 0 & 0 \\
0 & 0 & 0 & 0 & 0 & 0 & 0 & 0 & 1 & -1 & 0 & 0 & 0 & 0 & 0 & 0 & 0 & 1 & -1 \\
0 & 0 & 0 & 0 & 0 & 0 & 1 & -1 & 0 & 0 & 0 & 0 & 0 & 0 & 0 & 1 & -1 & 0 & 0 \\
0 & 0 & 0 & 0 & -1 & -1 & 1 & 1 & 0 & 0 & 0 & 0 & 0 & 1 & 1 & -1 & -1 & 0 & 0 \\
0 & 0 & 0 & 0 & 1 & -1 & 0 & 0 & -1 & -1 & 0 & 0 & 0 & -1 & 1 & 0 & 0 & 1 & 1 \\
0 & 0 & 0 & 0 & 0 & 0 & -1 & 1 & 1 & -1 & 0 & 0 & 0 & 0 & 0 & 1 & -1 & -1 & 1
\end{bmatrix}$$

can be achieved in many different ways and is still the subject of intensive research. As has been shown ([9]), the two-relaxation time (TRT) model yields results which are practically independent of the chosen viscosity. The TRT model used here can be seen as a derivative of the more general multi-relaxation time (MRT) model. The basic idea of the MRT model is to transform the distribution functions from the velocity space into the momentum space, carry out the collision step in the momentum space and afterwards transform the relaxed moments back into the velocity space. A LBM with a velocity space discretization of Q discrete velocities ξ_i has Q linearly independent moments (compare equation (5)). Since the moments are linearly independent, they can be relaxed at individual rates. If the function $\Psi(\xi)$ in equation (5) is chosen so that the corresponding moment represent a macroscopic property of the fluid, the relaxation time for this moment represents a physical property of the fluid. The density for example would not be relaxed at all in the case of an incompressible fluid. If the number of discrete velocities Q is higher than the number of linearly independent physical moments (13 in three dimensions) this can clearly not be done for all moments. The moments not representing a macroscopic property of the fluid can then be relaxed at a rate which can be freely tuned as to improve the numerical behaviour of the LBM. In the following, the MRT/TRT operator is described in detail.

If $\mathbf{R}$ is the vector containing Q linearly independent moments and $\mathbf{f}$ is the vector containing all the velocity distribution functions, a transformation matrix $\mathbf{M}$ exists which fulfils the following:

$$\mathbf{R} = \mathbf{M}\mathbf{f} \tag{10}$$

The momentum vector used in this paper is taken from [12] for the $D3Q19$ model and reads:

$$\mathbf{R} = \left[\rho, e, \varepsilon, j_x, q_x, j_y, q_y, j_z, q_z, 3p_{xx}, 3\pi_{xx}, p_{ww}, \pi_{ww}, p_{xy}, p_{yz}, p_{xz}, m_x, m_y, m_z\right]^T \tag{11}$$

where a Gram-Schmitt orthogonalization procedure was used to derive the 19 moments. The physical moments are the density ρ, the part of kinetic energy that is independent of the density e, the part of the kinetic energy square that is independent of the density and the kinetic energy $\varepsilon = e^2$, the momentum in the three spatial directions $\mathbf{j}$, the energy flux independent of the mass flux $\mathbf{q}$ and the symmetric viscous stress tensor $3p_{xx}, p_{ww} = p_{yy} - p_{zz}, p_{xy}, p_{yz}, p_{xz}$. Given the lattice links $\mathbf{e_i}$ according to (3), the transformation matrix $\mathbf{M}$ reads:

Using a diagonal matrix $\mathbf{S}$ with the diagonal elements $S_1, S_2 .., S_Q$, the collision step in momentum space can be written as

$$\tilde{\mathbf{R}} = \mathbf{R} - \mathbf{S}(\mathbf{R} - \mathbf{R}_{eq}) \tag{12}$$

where $\tilde{\mathbf{R}}$ describes the post collision state and $\mathbf{R}_{eq} = \mathbf{M}\mathbf{f}_{eq}$ is the vector of the moments of the discrete Maxwell distributions F_i. The diagonal elements of $\mathbf{S}$ are called the relaxation frequencies. In this paper the following relaxation frequencies are used:

$$diag(\mathbf{S}) = (0, 1.25, 1.25, 0, 0.89, 0, 0.89, 0, 0.89, 1.25, 1.25, 1.25, 1.25, 1.25, 1.25, 1.25, 0.89, 0.89, 0.89) \tag{13}$$

Since only two relaxation frequencies are used, the corresponding collision operator is also referred to as a two relaxation time operator. Once the collision, see equation (12), has been carried out, $\tilde{\mathbf{R}}$ has to be transformed to the velocity space again to complete the collision step.

2.4. Boundary Conditions

Four different boundary conditions (BC) are used in this study, namely the no-slip, velocity, pressure and symmetry BC.

No-slip BC: For no-slip boundaries the full bounce back (FBB) BC is employed. The FBB boundary condition is completely local and independent of the orientation of the boundary. These properties make this boundary condition very interesting for the simulation of flow through porous media, since all lattice nodes representing the solid matrix can simply be assigned the FBB boundary condition. It is easily observed that the FBB algorithm conserves mass whilst producing a zero velocity. It has been shown that the FBB boundary condition is only numerically accurate to first-order ([13-15]). Hence degrading the second-order accuracy of the LBM. Ziegler ([14]) as well as Zou and He ([13]) concluded that the FBB condition corresponds to a no-slip wall halfway between the row of fluid nodes and the row where the condition is applied. This conclusion is limited to simple geometries such as Couette or Poiseuille flow.

Velocity BC: The velocity boundary condition is implemented using the method proposed by Zou and He ([13]). This boundary condition is based on applying the bounce-back rule to the non-equilibrium parts of certain distribution functions. Using this BC, only the unknown velocity distribution functions are computed and the others are left untouched. Since the velocity is prescribed at the moving wall boundary, the density can be computed using the known distribution functions. The density of a boundary node can be split into three components. The first, ρ_-, is the sum of the unknown particle populations. The second, ρ_+, is the sum of the particle populations opposite to the unknown ones, and the third, ρ_0, sums up the particle populations whose lattice vector is tangential to the boundary or zero. Let $u_\perp$ be the projection of the macroscopic velocity onto the boundary normal pointing outside of the computational domain. Then, the particle density of the boundary node is given by

$$\rho = \rho_- + \rho_+ + \rho_0 \tag{14}$$

and the normal momentum is given by

$$\rho u_\perp = \rho_+ - \rho_- \tag{15}$$

Combining these equations yields the density as a function of the known distribution functions:

$$\rho = \frac{1}{1+u_\perp}\left(2\rho_+ + \rho_0\right) \tag{16}$$

Knowing the density and the velocity at the boundary allows us to compute the equilibrium distribution function f_{eq}. The non-equilibrium part of the known distribution functions f_{neq} can then be calculated:

$$f_{i,neq} = f_i - f_{i,eq} \tag{17}$$

In the following, the index $i+x$ identifies the lattice link pointing in the opposite direction to the one with the index i. All unknown distribution functions are now assigned a preliminary value in the following way:

$$f_i = f_{i,eq} + f_{i+x,neq} \tag{18}$$

In this manner, the exact value of the velocity component in the direction of the boundary normal is recovered. To keep this relation valid, the sum over the values of the unknown particle populations needs to be kept invariant during subsequent operations. The excess of momentum is then evaluated in the remaining directions tangential to the boundary. With the index t indicating the tangential direction and c representing the lattice vectors, the excess momentum E_t reads:

$$E_t = \sum_i f_{i,neq}\, c_{i,t} \tag{19}$$

The values E_t are then redistributed over the unknown distribution functions in order to achieve the desired momentum in all directions. Denoting the preliminary values for the unknown distribution functions as f_i', their final value can be expressed as follows:

$$f_i = f_i' - \sum_t \frac{1}{n_t} c_{i,t} E_t \tag{20}$$

where n_t denotes the number of unknown distribution functions for which the according lattice vector $c_{i,t}$ is non-zero. This concludes the streaming step at the boundary and is followed by the collision step.

Pressure BC: Prescribing the density instead of the velocity can also be achieved using the Zou and He boundary condition ([13]). In this case, equations (14) and (15) are used to determine the normal velocity at the boundary instead of the pressure, the tangential velocity components must be zero. The resulting equation for the normal velocity reads:

$$u_\perp = \frac{\left(2\rho_+ + \rho_0\right)}{\rho} - 1 \tag{21}$$

Now that the macroscopic velocity vector and the density are known, the distribution functions can be determined as in the case of the velocity boundary condition.

Symmetry BC: In the case of a symmetry boundary, the plane in which the boundary nodes lie is also a symmetry plane of the problem to be solved. Symmetry boundary conditions are very easy to implement. After streaming the unknown distribution functions at the boundary nodes are simply set to the values of the corresponding distribution functions on the other side of the symmetry plane.

3. DISCRETIZATION OF THE FIBRES

In this study, the centre-line of a fibre is always chosen to be at a lattice node. Therefore the discrete centre-line of a fibre that does not coincide with the Cartesian coordinates of the lattice is jagged. On all lattice nodes which are within the distance of the fibre radius r from the discrete centre line of

the fibre, the FBB boundary condition is enforced. In the following, the smallest radius which is necessary for a certain fibre discretization to be achieved is called the discretization radius r_d. As shown in Fig. (**1**), 19 possible discretizations of a circle exist if the discretization radius is chosen to be $r_d \leq 6$ lattice units.

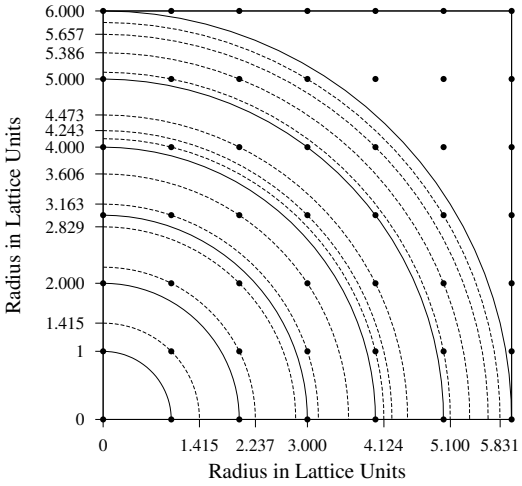

Fig. (1). Possible discretizations of a circle for discretization radii $r_d \leq 6$ lattice units. The dots represent lattice points and continuous and dashed lines represent the circles corresponding to the different discretization radii.

When discretizising fibres using the LBM in conjunction with the FBB-BC, two important factors have to be considered. Firstly, the exact location of the fluid-solid interface is located somewhere between the solid and the neighbouring fluid nodes. Where exactly the interface is modeled depends on the specific LBM scheme used and can not be influenced locally to adjust the interface location. In Ladd ([16]), the interface is assumed to be half way between the solid and neighbouring fluid nodes. In Fig. (**2**), the resulting geometry when discretizising a circle with a radius of 2.5 Lattice units is illustrated. In the following, the points at which the interface is effectively modeled are called boundary nodes. The exact location of the boundary nodes is

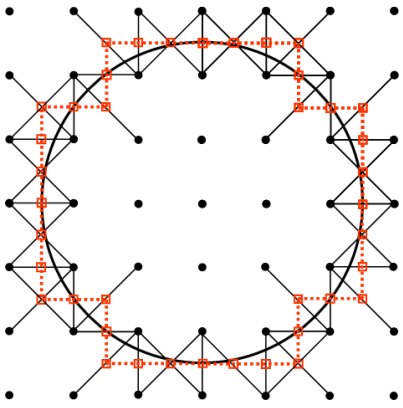

Fig. (2). Schematic cross-section of a fibre with a radius of 2.5 lattice units. Filled circles represent lattice nodes and red squares represent boundary nodes. All nodes within the circle are solid nodes and the remaining nodes are fluid nodes. Lattice links connecting fluid- and solid-nodes are shown as lines with the boundary nodes at their centers. The red dotted line describes the resulting geometry that is effectively discretizised.

not known for the LBM used here but the geometric observations presented in this paragraph hold true as long as the boundary nodes are located a constant fraction of the lattice link away from the solid nodes. Due to this uncertainty, the modeled geometry is not well defined. It is convenient to define a reference geometry that can be uniquely associated with a certain discretization. In the case of fibres considered here, the previously introduced discretization radius r_d is chosen to describe the reference geometry. Secondly, curved fluid-solid interfaces can only be approximated by a jagged interface when using the FBB boundary condition, as can be seen in Fig. (**2**). Following the example given in Fig. (**2**), the resulting geometries that are represented by the the different discretizations considered here can be obtained and are depicted in Fig. (**3**). It can be seen that an increase in discretization radius does not necessarily result in a better geometric representation of a circle. When the discretization radius is chosen to be 0, 1.415 or 2.829 for example, then effectively the discretizised geometry is a square. As a measure of how well a certain discretization describes the fibre it represents, the following volume ratio is introduced:

$$VR = \frac{V_f}{V_d} \tag{22}$$

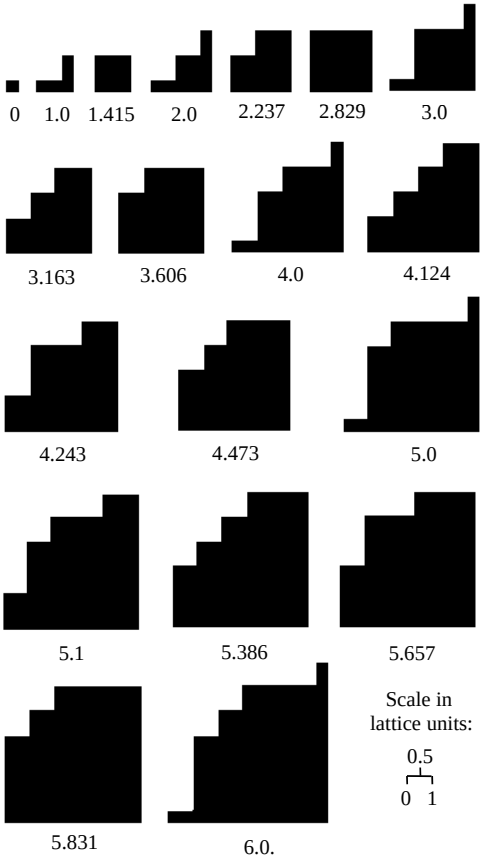

Fig. (3). Effectively modeled geometries for all discretization radii $r_d \leq 6$ when assuming the boundary nodes to be half way between the fluid- and solid nodes.

where V_f is the volume of the fibre to be discretizised and V_d is the volume enclosed by the surface connecting the

boundary nodes as illustrated in Fig. (**2**). Furthermore a radius r_{VR} is defined which fulfils the relationship $V_d = \pi \cdot r_{VR}^2$. The VR for the discretization radii considered in this paper are listed in Table **1**.

4. GENERATION OF RANDOM FIBROUS POROUS MEDIA

In this paper two types of random fibrous porous media are investigated, namely the random array of parallel cylinders and the random disordered array of cylinders. For the simulations, cubic samples of the porous media are created. In the case of the random array of parallel cylinders, a lattice point within the sample domain is randomly chosen which represents a point on the centerline of one of the fibres. The fibre is then discretizised according to paragraph 4. This procedure is repeated until the required SVF is achieved. The SVF is related to the porosity ε_p of a porous medium in the following way:

$$SVF = 1 - \varepsilon_p . \tag{23}$$

In the case of the random disordered arrays of cylinders, a point on the centerline, the angle α between the fibre and the x-z-plane and the angle β between the fibre and the x-y-plane are randomly chosen. The fibre is then discetizised according to paragraph 4. The process is repeated until the required SVF is achieved. Overlapping of fibres is possible employing the approaches for geometry creation described here.

Table 1. Table of all Discretization Radii r_d Considered in this Paper Together with the Corresponding Volume ratio VR and the Effective Hydrodynamic Radii r_h Obtained Via the Calibration Process

r_d	r_h	VR
1.000	1.257799253	0.628
1.415	1.575406821	0.699
2.000	2.177106122	0.967
2.237	2.527603649	0.749
2.829	2.771143826	1.006
3.000	3.154686881	0.975
3.163	3.484259055	0.849
3.606	3.723425773	0.908
4.000	4.079299929	1.026
4.124	4.395236807	0.937
4.243	4.456854462	0.927
4.473	4.666210863	0.911
5.000	5.141047012	0.970
5.100	5.406455984	0.918
5.386	5.404980687	0.940
5.657	5.671614683	0.995
5.831	5.837739421	0.980
6.000	6.102821297	1.001

5. CALIBRATION OF THE LBM

On coarse numerical lattices, both the uncertainty of the location of the solid-fluid interface and the jagged shape of the fibre-discretizations r_d are expected to have a significant impact on the predicted permeability. Assuming an unimodal fibrous medium with the fibre radius r_d and the LBM representation of that medium being discretizised using r_d, the difference between a characteristic property R of the flow through that medium and the value of that property as predicted by the LBM can be divided as follows:

$$R - R_{LB} = \Delta R_U + \varepsilon_{D,J} + \varepsilon_r \tag{24}$$

Here ΔR_U is the difference between the predicted and the correct value of R due to the uncertainty of the solid-fluid boundary location, $\varepsilon_{D,J}$ is the error due to the jaggedness of the curved boundaries and ε_r represents all other error terms. On coarse numerical lattices, the first two terms in equation (24) are expected to be dominant and hence $\Delta R_U + \varepsilon_{D,J} >> \varepsilon_r$, with the exception of flows through narrow channels. In the latter case the spacial discretization of the channel is likely to be less than two lattice units, in which case the LBM is known to yield significant discretization errors. In the case of unimodal fibrous porous media, ΔR_U is expected to be independent of the fibre arrangement considered, since every fibre is discretizised in the same way. $\varepsilon_{D,J}$ on the other hand is not, since the difference between the actually modeled geometry and the desired geometry due to the jaggedness has different hydrodynamic effects for different fibre arrangements in general. With increasing distance from a fibre, the effect of a fibre on the flow is less dependent on the actual cross-section of that fibre. Therefore, in the special case of low SVFs, $\varepsilon_{D,J}$ is assumed to be constant. Following the above assumptions, $\Delta R_U + \varepsilon_{D,J}$ can be estimated by carrying out computations for hydrodynamic problems where the solution is known and can be accounted for in subsequent predictions. The procedure of determining $\Delta R_U + \varepsilon_{D,J}$ can therefore be considered as a calibration process of the LBM for a specific type of geometry and its discretization. This calibration process is carried out for the different fibre discretizations depicted in Fig. (**3**).

The benchmark problem employed here is the flow through a square array of parallel cylinders. The geometry of the problem is uniquely defined by the SVF C, which is a function of the cylinder radius r:

$$C = \frac{\pi \cdot r^2}{L^2} \tag{25}$$

where L is the shortest distance between two cylinders to be found in the array. The characteristic parameter of the flow is

chosen to be the non-dimensional drag force F_{ND} on a single cylinder in the array. F_{ND} can be computed from the LBM results in the following way:

$$F_{ND,LB} = \frac{\Delta p \cdot A}{\bar{U} \cdot \nu \cdot l} \tag{26}$$

where Δp is the average pressure drop between two neighbouring symmetry planes perpendicular to the main flow direction, A is the the cross-sectional area for a repeat element, U is the volume averaged velocity in the main-flow direction, ν is the lattice viscosity and l is the length of the cylinders which is choosen to be unity throughout this paper. The results obtained using the LBM are compared with the literature data to obtain an estimate for $\Delta R_U + \varepsilon_{D,J}$. At volume fractions of $C = 0.2$ and less, the analytical expression for dilute arrays $C = 1$ proposed by Sangani and Acrivos ([17]) to obtain the non-dimensional drag force F_{ND} is used for comparison:

$$F_{ND} = F_{ND}(C) = F_{ND}(r^2) = \frac{F}{\bar{U}\nu l} = \frac{4\pi}{\ln \cdot C^{1/2} - 0.738 + C - 0.887C^2 + 2.038C^3 + 0C^4} \tag{27}$$

where F is the dimensional drag force. At higher SVFs this expression is not accurate and the computational results of Sangani and Acrivos ([17]) are used for comparison. To be able to easily apply the obtained results for $\Delta R_U + \varepsilon_{D,J}$ to other fibrous geometries, it is expressed using the idea of an effective hydrodynamic radius r_h. Using the LBM results and the literature data for F_{ND}, the effective hydrodynamic radius r_h can be defined so that the following relation is satisfied:

$$F_{ND,LB} = F_{ND}(r_h^2) = F_{ND}(r_d^2) + \Delta R_U + \varepsilon_{D,J} + \varepsilon_r \tag{28}$$

It is worth noting that the choice of r_d as a reference radius has some implications on the interpretation of δr. Since r_d is defined as the smallest possible radius to achieve a certain discretization and the actual boundary is known to lie somewhere between the solid nodes and their neighbouring fluid nodes, the difference of the two radii $\delta r = r_h - r_d$ is likely to be positive.

In Fig. (**4**), the difference between the discretization radius and the effective hydrodynamic radius, δr, is shown as a function of the discretization radius r_d for different SVFs C, $C = C(r_d)$. For certain combinations of r_d and C, no meaningful LBM solution can be obtained since the gap between the cylinders reduces to one lattice unit and this is insufficient to model the flow in the gap. The results obtained show that the determined values of r_h for different SVFs are clearly correlated. This supports the assumption that the error in the LBM is dominated by $\Delta R_U + \varepsilon_{D,J}$ and it is relatively independent of the considered fibre arrangement. To further illustrate this assumption, more complex problems have to be considered since all cases considered here involve relatively similar arrangements. another interesting detail is that δr correlates very well with $\delta r_{VR} = r_{VR} - r_d$, which suggests that the SVF of the modeled medium is of much higher importance than the actual cross-section of the modeled fibre.

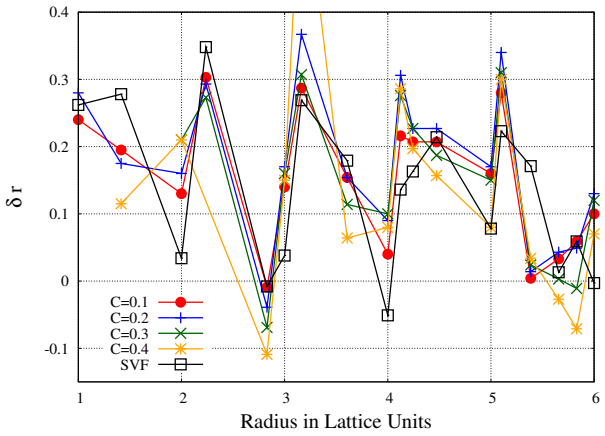

Fig. (4). The difference between discretization radius and hydrodynamic radius, $\delta r = r_h - r_d$, as a function of the discretization radius r_d for different SVFs C. The SVFs are based on the discretization radius r_d. In addition $\delta r_{VR} = r_{VR} - r_d$ is presented.

6. PERMEABILITY PREDICTIONS FOR RANDOM FIBROUS GEOMETRIES

Two different geometries are investigated, namely a random array of parallel cylinders and a random disordered array of cylinders. Since, in the former case the problem can be reduced to two dimensions, it is referred to as the 2D case and the latter problem is referred to as the 3D case. Taking into account the findings of the previous section, the discretization radius r_d is chosen in a way so that the associated effective hydrodynamic radius r_h matches the desired fibre radius. The actual porous medium being modeled is of square or cubic shape for the 2D and 3D cases, respectively. The length of the edges l of the porous domain are chosen to be $100 \times r_h$ for the 2D case and $50 \times r_h$ for the 3D case. According to previous studies ([18]) the chosen domain sizes are large enough to obtain a result which is sufficiently statistically independent. In the main flow direction, the domain extends a distance S to both sides of the porous medium. The chosen boundary conditions are the same for the 2D and 3D cases and are illustrated in Fig. (**5**). In the 2D case, the geometry was created in such a way that the fibres do not intersect. This restriction was not applied in the 3D case. Due to limited computational resources, computations were only carried out for discretization radii up to $r_d = 4$ lattice units for the 3D case. Furthermore, no converged results were obtained for the 2D case at a SVF of $C =$ 0.4. The non-dimensional permeability k is chosen as the reference parameter and is defined as follows:

$$k = \frac{\bar{U}\nu}{\Delta p \cdot t_m \cdot a^2} \tag{29}$$

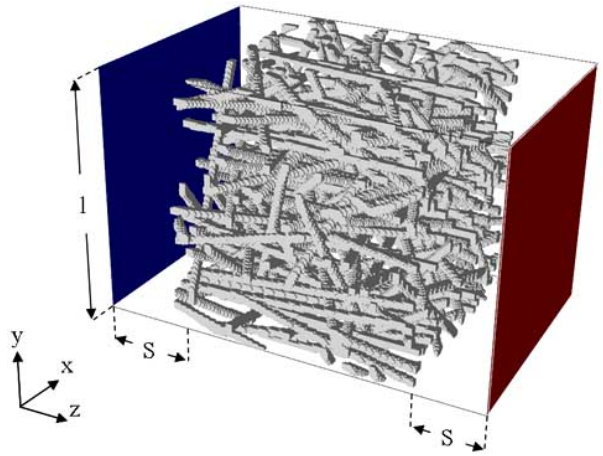

Fig. (5). Schematic of the boundary conditions employed for the permeability predictions. The blue and red surfaces represent the inlet and outlet boundaries, respectively. At the inlet a uniform velocity in the positive z-direction is enforced while a uniform pressure is enforced at the outlet. The other boundaries confining the computational domain are symmetry boundary conditions. S denotes the distance from the porous medium to the inlet or outlet boundaries. l denotes the size of the square (2D case) or cubic (3D case) sample of the porous medium.

where t_m is the thickness of the porous medium in the main flow direction in lattice units and a is the fibre radius in lattice units which is used to make the permeability non-dimensional. Here, t_m equals l and a equals r_h.

The results obtained using the LBM are compared to the results obtained by Sangani and Mo ([19]) in the 2D case and with the results of Clague *et al*. ([4]) in the 3D case. In Sangani and Mo ([19]) the results are presented in the form of a scaled average force per cylinder. It is transformed into the above definition of k as follows:

$$k = \left(\frac{F}{4\pi\nu\bar{U}} \right)^{-1} \cdot \frac{1}{4\pi r^2} \tag{30}$$

where the term in the brackets on the right hand side represents the results as given in ([19]) and r^2 is obtained as follows:

$$r^2 = \frac{C}{\pi} \tag{31}$$

The data taken from ([19]) is in very good agreement with the results obtained by other authors ([20] and references therein). The results presented in Clague *et al*. ([4]) are for different SVFs than the ones considered in this paper and the required values are obtained by manual interpolation. Results for the permeability of random disordered fibrous porous media vary considerably ([21]) and have to be interpreted with care. All literature data that is used for comparison in this paper is summarised in Table **2**.

The total error E, as calculated with the literature values for the permeability k_L and the corresponding LBM result k_{LB} is expressed as a percentage of the literature value. A negative error indicates an overprediction of the permeability and the converse argument is true. In Fig. (**6**) the error is depicted for the different discretizations and for different SVFs for both the 2D and the 3D case. Since the calibration process aimed at compensating for ΔR_U and $\varepsilon_{D,J}$, E is the residual error ε_r plus an error ε_c which represents the error due to the limited applicability of the assumptions made during the calibration process. In general the residual error ε_r is expected to decrease monotonically with increasing lattice resolution.

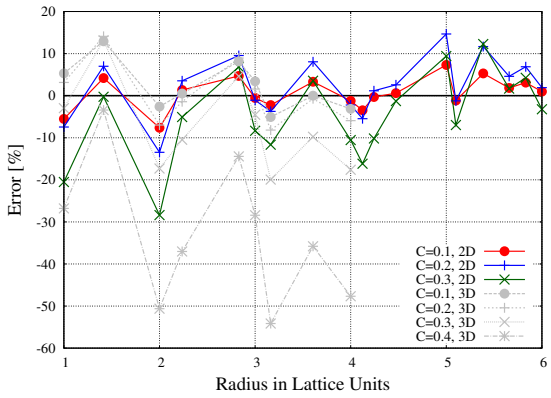

Fig. (6). The error E of the LBM predictions of the hydraulic permeability as a function of the discretization radius r_d for different SVFs and different geometries. The 2D case refers to a random array of parallel cylinders while the 3D case refers to a random disordered porous medium.

It can be seen that the error, as a function of the discretization radius $E = E(r_d)$, is alternating and is correlated for all considered cases. Due to the calibration process, the error does not decrease monotonically with the lattice refinement. With the exception of the 3D cases with a SVF of 0.4, E alternates around 0 and the amplitude decreases slightly with increasing discretization radius. Since ε_r is expected to decrease monotonically with the lattice resolution, the alternating behaviour of E can be attributed to the limited applicability of the assumptions made during the calibration process.

Table 2. Literature Data for the Non-Dimensional Permeability k for the Different SVFs C. Data Taken from [19] and [4]. In the Last Line the Error $\varepsilon_{a,abs}$ Obtained in this Paper is Presented for the Different SVFs

C	0.1	0.2	0.3	0.4
k, S & M, 2D	1.667	0.338	0.094	N/A
k, Clague, 3D	2.15	0.71	0.27	0.102
$\varepsilon_{a,abs}$[%]	3.6	5.8	9.7	33.1

The assumption of $\varepsilon_{D,J}$ being sufficiently independent of the structure of the fibrous medium is only valid if the distance between the fibres is large enough. With increasing SVF this assumption becomes less valid and therefore ε_c is expected to increase. With increasing SVF, the fluid channels become narrower and are therefore represented by fewer fluid nodes. This leads to an expected increase in ε_r. In Table **2** the absolute value of the error, averaged over all discretizations, $\varepsilon_{a,abs}$ is presented and indeed increases with increasing SVF. While both components of E are expected to increase with C, they can affect the result contrarily. This observation can explain why, for certain discretizations, the absolute error is not increasing with the SVF.

The aim of this paper is to improve the accuracy of the LBM in predicting the permeability of fibrous porous media when using coarse numerical lattices. In Fig. (**7**) the total error of the non-calibrated LBM is presented for a square array of parallel cylinders. In this case, the effective hydrodynamic radius r_h was chosen to be equal the discretization radius r_d. For the square array of parallel cylinders the SVF is a function of the distance L between the center lines and the cylinder radius r (compare equation (25)). Since in the LBM L is an integer value, the possible SVFs that can be modeled using a certain discretization radius are finite. For this reason only certain data points are included in Fig. (**7**). To determine the error the LBM results were compared with the data obtained by Sangani and Acrivos ([17]). Comparing Figs. (**7**) and (**6**) it can be observed that the calibration process did, in general, not improve the accuracy of the LBM at fibre discretisations of $r_d \geq 4$. In the non-calibrated case, the error strongly increases for smaller discretization radii while the amplitude of $E(r_d)$ increases only moderately.

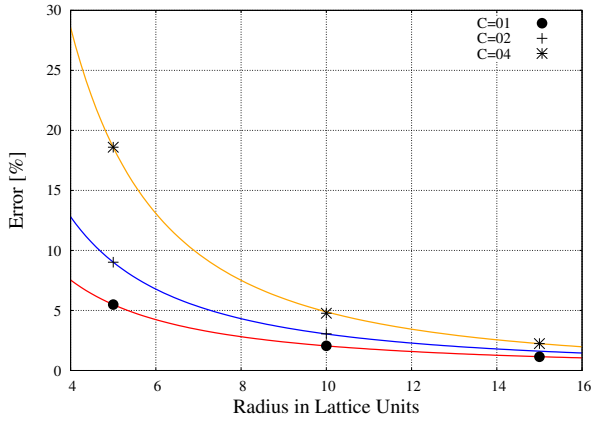

Fig. (7). The total error of the LBM predictions of the hydraulic permeability of a square array of parallel cylinders as a function of the discretization radius r_d for different SVFs. The solid lines are regressions of the point data. For these computations r_h is set equal to r_d.

CONCLUSIONS

The calibration process employed in this paper is able to significantly improve the accuracy of the LBM for the special case of fibrous porous media when using very small discretization radii $r_d \leq 4$. At moderate discretization radii of $4 \leq r_d \leq 6$ the calibration process does not generally have a positive effect on the results. For SVFs ≤ 0.2 the calibration process offers the possibility to significantly reduce the computational cost if an error of about 10-15% is acceptable. At higher SVFs the error significantly increases and makes the use of coarse lattices questionable. Since the error as a function of the discretization radius alternates around 0 for SVFs $\leq$ 3, the accuracy of the LBM can be improved by carrying out several computations on coarse lattices and averaging the results.

ACKNOWLEDGEMENTS

The authors would like to thank for the financial support provided by the European Union Marie Curie Fellowship Programme as well as the Centre for CFD in the University of Leeds.

NOMENCLATURE

Roman Letters

A	=	Area
c_S	=	Lattice speed of sound
C	=	Solid volume fraction
E	=	Error term
E_t	=	Excess momentum
f_i	=	Discrete velocity distribution function
F_i	=	Discrete equilibrium distribution function
F_{ND}	=	Force on a single cylinder
k	=	Non-dimensional permeability
m	=	Moment of the distribution function
n_t	=	Number of unknown distribution functions
p	=	Lattice pressure
Q	=	Number of velocity vectors
R	=	Characteristic property
r_d	=	Discretization radius
r_h	=	Effective hydrodynamic radius
t	=	Time
t_m	=	Material thickness
$\bar{U}$	=	Volume averaged lattice velocity
VR	=	Volume ratio
w_i	=	Weigthing factor

Greek Letters

α	=	Fibre angle
β	=	Fibre angle
ε_p	=	Porosity
ε_r	=	Error term
$\varepsilon_{D,J}$	=	Error term
ν	=	Lattice viscosity

ρ = Lattice density

τ = Relaxation rate

Ω = Collision operator

Ψ = Momentum ansatz

Vectors and Tensors

$\mathbf{e_i}$ = Lattice link

$\mathbf{f}$ = Vector containing distribution functions

$\mathbf{M}$ = Transformation matrix

$\mathbf{r}$ = Particle position vector

$\mathbf{R}$ = Momentum vector

$\tilde{\mathbf{R}}$ = Momentum vector, post collision state

$\mathbf{R_{eq}}$ = Equilibrium momentum vector

$\mathbf{S}$ = Relaxation matrix

$\mathbf{u}$ = Macroscopic velocity vector

ξ_i = Particle velocity vector

Abbreviations

BC = Boundary condition

BGK = Baghnar-Gross-Krook

FBB = Full bounce back

LU = Lattice unit

LBM = Lattice Boltzmann method

MRT = Multiple relaxation time

SRT = Single relaxation time

SVF = Solid volume fraction

TRT = Two relaxation time

REFERENCES

[1] S. Zobel, B. Maze, H. Vahedi Tafreshi, Q. Wang, and B. Pourdeyhimi, "Simulating permeability of 3-D calendered fibrous structures", *Chem. Eng. Sci.*, vol. 62, no. 22, pp. 6285-6296, 2007.

[2] L. Clarenburg and R. Werner, "Aerosol Filters. Pressure Drop across Multicomponent Glass Fiber Filters", *Ind. Eng. Chem. Process Des. Dev.*, vol. 4, no. 3, pp. 293-299, 1965.

[3] S. Jaganathan, H. Vahedi Tafreshi, and B. Pourdeyhimi, "A realistic approach for modeling permeability of fibrous media: 3-D imaging coupled with CFD simulation", *Chem. Eng. Sci.*, vol. 63, no. 1, pp. 244-252, 2008.

[4] D. Clague, B. Kandhai, R. Zhang, and P. Sloot, "Hydraulic permeability of (un) bounded fibrous media using the lattice Boltzmann method", *Phys. Rev. E*, vol. 61, no. 1, pp. 616-625, 2000.

[5] D. Koch and A. Ladd, "Moderate Reynolds number flows through periodic and random arrays of aligned cylinders", *J. Fluid Mech.*, vol. 349, pp. 31-66, 1997.

[6] M. Van Doormaal and J. Pharoah, "Determination of permeability in fibrous porous media using the lattice Boltzmann method with application to PEM fuel cells", *Int. J. Num. Meth. Fluids*, vol. 59, no. 1, 2009.

[7] J. Ferziger and M. Peri´c, *Computational methods for fluid dynamics*. Springer: New York, 1999.

[8] D. Wolf-Gladrow, *Lattice-gas cellular automata and lattice Boltzmann models: an introduction*. Springer: Verlag Berlin, 2000.

[9] C. Pan, L. Luo, and C. Miller, "An evaluation of lattice Boltzmann schemes for porous medium flow simulation", *Comput. Fluids*, vol. 35, no. 8-9, pp. 898-909, 2006.

[10] D. H¨anel, *Molekulare Gasdynamik*. Springer: Berlin 2004.

[11] S. Chen and G. Doolen, "Lattice Boltzmann method for fluid flows", *Ann. Rev. Fluid Mech.*, vol. 30, no. 1, pp. 329-364, 1998.

[12] D. d'Humi`eres, I. Ginzburg, M. Krafczyk, P. Lallemand, and L. Luo, "Multiple-relaxation-time lattice Boltzmann models in three dimensions", *Philos. Trans. Math. Phys. Eng. Sci.*, pp. 437-451, 2002.

[13] Q. Zou and X. He, "On pressure and velocity flow boundary conditions and bounceback for the lattice Boltzmann BGK model", *Arxiv preprint comp-gas/9611001*, 1996.

[14] D. Ziegler, "Boundary conditions for lattice Boltzmann simulations", *J. Stat. Phys.*, vol. 71, no. 5, pp. 1171-1177, 1993.

[15] R. Cornubert, D. d'Humieres, and D. Levermore, "A Knudsen layer theory for lattice gases", *Phys. D*, vol. 47, pp. 241-259, 1991.

[16] Ladd, "Numerical simulations of particulate suspensions via a discretized Boltzmann equation. Part 2. Numerical results", *J. Fluid Mech. Digital Arch.*, vol. 271, pp. 311-339, 2006.

[17] A.S. Sangani and A. Acrivos, "Slow flow past periodic arrays of cylinders with application to heat transfer", *Int. J. Multiphase Flow*, vol. 8, no. 3, pp. 193-206, 1982.

[18] M. L. R. Thomas, D. B. Ingham, and M. Pourkashanian, "Prediction of permeabilities of gas diffusion layers of fuel cells using the lattice Boltzmann method", *Proceedings of 4th ICAPM*, 2009.

[19] A. S. Sangani and G. Mo, "Inclusion of lubrication forces in dynamic simulations", *Phys. Fluids*, vol. 6, p. 1653, 1994.

[20] R. Hill, D. Koch, and A. Ladd, "Moderate-Reynolds-number flows in ordered and random arrays of spheres", *J. Fluid Mech.*, vol. 448, pp. 243-278, 2001.

[21] M. Tomadakis and T. Robertson, "Viscous permeability of random fiber structures: comparison of electrical and diffusional estimates with experimental and analytical results", *J. Comp. Materials*, vol. 39, no. 2, p. 163, 2005.

Received: August 06, 2009 Revised: March 15, 2010 Accepted: March 16, 2010